Earthq Eng & Eng Vib (2018) 17: 355-369 **DOI**: https://doi.org/10.1007/s11803-018-0446-9

Seismic performance of interior precast concrete beam-column connections with T-section steel inserts under cyclic loading

Rattapon Ketiyot[1†] and Chayanon Hansapinyo[2‡]

1. *Department of Civil Engineering, Chiang Mai University, 239 Heay-Kaew Rd., Suthep, Muang, Chiangmai 50200, Thailand*
2. *Center of Excellence for Natural Disaster Management, Chiang Mai University, 239 Heay-Kaew Rd., Suthep, Muang, Chiangmai 50200, Thailand*

Abstract: An experimental investigation was conducted to study the performance of precast beam-column concrete connections using T-section steel inserts into the concrete beam and joint core, under reversed cyclic loading. Six 2/3-scale interior beam-column subassemblies, one monolithic concrete specimen and five precast concrete specimens were tested. One precast specimen was a simple connection for a gravity load resistant design. Other precast specimens were developed with different attributes to improve their seismic performance. The test results showed that the performance of the monolithic specimen M1 represented ductile seismic behavior. Failure of columns and joints could be prevented, and the failure of the frame occurred at the flexural plastic hinge formation at the beam ends, close to the column faces. For the precast specimens, the splitting crack along the longitudinal lapped splice was a major failure. The precast P5 specimen with double steel T-section inserts showed better seismic performance compared to the other precast models. However, the dowel bars connected to the steel inserts were too short to develop a bond. The design of the precast concrete beams with lap splice is needed for longer lap lengths and should be done at the beam mid span or at the low flexural stress region.

Keywords: precast concrete; beam-column connection; cyclic loading

1 Introduction

Earthquakes are natural disasters that have the potential to devastate and destroy cities. Efforts are being made to mitigate or minimalize this damage. Earthquake resistant buildings are imperative to prevent buildings from collapsing and causing subsequent financial losses. The northern, western and middle regions of Thailand have been designated as seismic zones equivalent to a moderate seismic zone; specifically, seismic zones 2A-2B according to UBC design provisions (1997). The region has been declared a seismic zone based on the geological evidence and past earthquake records. Mid-year 2014, an earthquake with a magnitude of 6.3, the biggest earthquake to have occurred in Thailand, struck the Chiang Rai province located in northern-Thailand, causing severe damage to numerous concrete buildings.

Most buildings in Thailand have been constructed using a traditional cast-in-place system. However, the system is being replaced by one that is prefabricated due to the reduction of construction time. The precast construction offers several advantages, such as better quality control and lower overall construction costs. Normally, the performance of precast concrete structures is influenced by the quality of their connections. From previous studies, most damage and abrupt failures of precast concrete structures during earthquakes was mainly due to the failure of joint assembly and inadequate ductility. There were several investigative studies showing the importance of ductile connections in precast structures (Arslan *et al.*, 2006; Chayanon *et al*., 2017; Gülkan, 1998 and Park, 2002). To design a precast connection, PCI standards have been widely adopted as a standard design guideline. However, the most explicit precast connection detailing from the PCI manual (1973) and handbooks (2010) was designed specifically to support the gravity load rather than the lateral load. The current precast connections used in seismic areas have been adopted from in-house research information. Hence, despite the many advantages of precast concrete, it has not been widely adopted due to concern about its seismic performance and building stability during strong ground motions.

The NEHRP Provision (1998) described two alternative precast connection designs for a lateral load resisting system. One is a monolithic reinforced concrete emulation exhibiting rigid-elastic behaviors, while the other is a precast concrete connection with unique performance that allows certain deformations. Gosh *et al.* (1997) illustrated precast concrete connection designs

Correspondence to: Chayanon Hansapinyo, Center of Excellence for Natural Disaster Management, Chiang Mai University, 239 Heay-Kaew Rd., Suthep, Muang, Chiangmai 50200, Thailand
Tel: 66-53-944175; Fax: 66-53-942044
E-mail: chayanon@eng.cmu.ac.th
[†]Doctoral student; [‡]Associate Professor

Received August 23, 2016; **Accepted** December 9, 2016

based on the high seismic regions described in the 1997 UBC provisions. The connections were designed to remain elastic, while the connecting elements behaved nonlinearly. To avoid connection failure, the connection capacity must be higher than the plastic moment capacity of the beams. When the location of the plastic hinge on the beam moved further away from the connection they exhibited better seismic performance.

There have been several researchers who have made new discoveries about precast concrete connections in the last decade. Kormaz and Tankut (2005) investigated the seismic behavior of the precast concrete beam-to-beam connections with welded plates, and concluded that the improved connection details could be suitably used for seismic structures. Yang *et al.* (2010) developed hybrid precast concrete beams with H-steel beams at both ends to create a simple ductile connection, which is particularly useful for precast concrete structures. Three precast concrete beams were tested under two-point concentrated loads to explore the effectiveness and limitations of the developed hybrid beam system in transferring an applied load to a supporting column. The results showed that the introduction of a pre-stressing force in longitudinal tension reinforcement significantly improved the flexural capacity and ductility of the hybrid precast concrete beams.

Regarding studies of beam-column precast connections in moment-resisting frames, Ertas *et al.* (2006) studied the performance of four ductile precast concrete connections, and a monolithic connection for moment resisting frames under reversed cyclic loading. The test results showed that the strength and energy dissipation could be suitable for high seismic zones. Li *et al.* (2009) studied the seismic performance of precast hybrid-steel concrete connections under cyclic loading. The experimental observations showed the precast connections without abrupt damage within the joint core region, exhibiting adequate ductile behavior and were considered acceptable in comparison to the monolithic one. Embedment of the steel sections in the joint greatly enhanced the strength of the joint-core leading to an increase of the ductility factor to 3.50. Ketiyot and Hansapinyo (2012) studied the seismic resistance of the exterior precast concrete beam-column frame using a combined welded-bolted connection. The seismic performance was compared to the monolithic one under cyclic loading. The precast beam was connected to the precast column at the column face. The test results indicated that the precast specimen showed better seismic performance including; ultimate capacity, ductility, and energy dissipation capacity. Hansapinyo (2012) observed an experimental investigation of the exterior cast-in-place and welded precast concrete frames under cyclic loading; one precast and two monolithic specimens were tested. The difference between the two monolithic specimens was the reinforcement in the beam–column joint regions; e.g. with and without transverse reinforcement. Test results showed that the precast specimens performed better hysteretic responses, higher stiffness, and lower joint distortion. This was due to the additional embedded steel plates. The connecting purpose increased the resistance of the diagonal crack growth in the joint area. Vidjeapriya and Jaya (2013) presented the experimental results of two precast concrete beam-column connections compared to the monolithic connection under cyclic loading. The precast beam was connected to the column with a corbel using a cleat with a single stiffener for the first precast specimen, and double stiffener for the second specimen. The test results revealed that the ultimate loading of the monolithic specimen was better than the other precast specimens. The energy dissipation and ductility of both precast specimens exhibited satisfactory behavior. In a similar study, Shariatmadar and Zamani Beydokhti (2014) investigated the seismic response of three precast interior subassemblies to compare with a monolithic connection. All precast joints were assembled by using cast-in-place connections with different details; namely straight sliced, U-shaped, and U-shaped with a steel plate. Comparisons of seismic performance showed that the seismic performance of the precast specimen with straight sliced and the monolithic specimen were similar and can be suitable for use in high seismic zones. Wongmatar *et al.* (2015) proposed the detailing of these reinforcements in the interior beam–column connections, aiming to relocate the plastic hinge of the monolithic reinforced concrete, and precast concrete frames with T-section steel inserts embedded into the concrete connection. Four specimens, including two monolithic specimens, and two precast ones, were tested under cyclic loading. The test results showed that the crack patterns of the precast specimens were generated at the end of the steel insert connections. However, slipping of the lap splices at the top of the beam section were observed before the yielding of the bars, which ultimately led to the brittle fracture. Furthermore, the diagonal bars inserted into the precast joint improved the seismic performance; i.e. initial stiffness and energy dissipation.

Xue and Yang (2010) reported the results of their experimental investigations on four full-scale precast concrete beam–column connections, and a half-scale moment-resisting frame. The frame was two-bay, two-story high precast concrete, which included exterior connections, interior connections, T-connections and knee connections. The test results revealed that the precast concrete connections and frames could perform effectively in seismic conditions with respect to strength, ductility, and energy-dissipation capacity. A new ductile moment-resisting beam-column connection was developed by Parastesh *et al.* (2014) for precast reinforced concrete frames to be used in high seismic zones. Six full-scale interior and exterior precast connections, and two monolithic connections, were subjected to a reverse cyclic loading. It was concluded that the proposed precast connections proved to be effective at improving the seismic performance, and also provided adequate flexural strength, strength

degradation, and drift capacity. Moreover, Tsonos *et al.* (1992), Au *et al.* (2005), Chalioris *et al.* (2008) and Lu *et al.* (2012) conducted experimental investigations of diagonal reinforcement embedded into the beam-column concrete joints to reduce the force transferred to the joint core. The test results showed that joints, with crossed and inclined reinforcements, demonstrated improved seismic performance. Furthermore, in terms of overall cracking observations, the specimens with diagonal bars showed fewer cracks in the column when compared to the specimens without them. Regarding bond behavior of deformed bar to concrete, there was a study (Soroushian *et al*., 1991) describing the effect of compressing strength of concrete to bond splitting behavior. The bond strength increases with increasing compressive strength. For the bond stress and slip values of the bond stress-slip relationship, the test result showed that the bond stress of strength concrete over 50 MPa rapidly decreased after peak bond strength. However, this characteristic was not consistently influenced by variations in concrete strength. That was similar to a study by Diab *et al.* (2014), which investigated the bond behavior of normal and high strength concrete. The test results revealed that high strength concrete specimens failed in a brittle mode. Furthermore, failure of the specimens was abrupt due to forming longitudinal splitting cracks.

From the literature above, one may ascertain that the precast connection details play an important role in withstanding lateral load and there have been many types of precast concrete connections, all of which have been developed for different purposes; to obtain a seismic capacity of precast concrete connections compared to traditional monolithic connections, and to improve displacement ductility factors of precast structures that have undergone earthquake loading. This study was also aimed at the development of a precast concrete connection suitable for use in Thailand and for moderate earthquake capacity. A T-section steel insert in a beam embedded in the precast beam ends is the system proposed as an extension of previous work (Wongmatar *et al.*, 2015). It helps the fabrication process by ignoring the shoring system as the protruded part of the T-section steel can be seated on the column edge (as shown in Fig. 1). The depth of the top beam was dropped to install lap-splice bars for connecting both beams through the beam-column joint. The study presents test results for six 2/3-scale concrete beam–column interior subassemblages, including one monolithic and five precast connections. The monolithic connection was seismically designed based on ACI318-14 (2014) as the reference specimen. The five precast specimens were designed with different connection details.

2 Experimental program

A 4-6 story building prototype (such as an office building) was represented in this study. The height of each story was 3.50 m, and the bay width was 4.50 m. The beam and column sizes were determined for width/depth dimensions as 300/450 mm and 200/450 mm, respectively. NEHRP: Seismic design technical brief No.1 (2008) suggested that a beam flexural reinforcement in the joint region should be 0.01, stating that it is more practical for constructability. Furthermore, a column reinforcement ratio was in excess 0.03. Therefore, the beam reinforcement ratios at the top and bottom regions were 0.0116 and 0.0086, respectively. The reinforcement ratio of the column was also 0.0118.

This study conducted a test on six interior beam-column concrete specimens, which were divided into one monolithic and five precast concrete connections

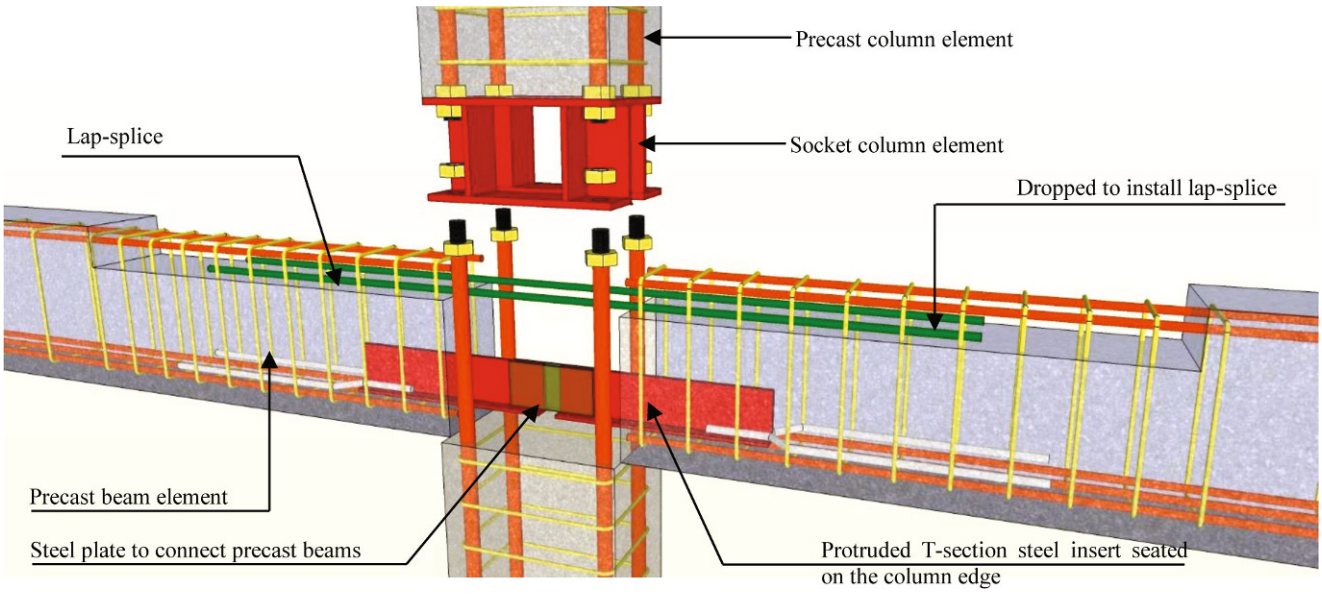

Fig. 1 Precast beam element with T-section steel insert

using T-section steel inserts embedded into the core of the beam-column joint. The strong column-weak beam theory was applied in the design of all specimens. They were scaled to approximately 2/3 of the usual beam-column frame element in the prototype buildings, because the acceptable minimum limit scaling factor is 1/3 full size in the ACI T1.1-01 document (2001). Test specimens were planar beam -column subassemblies representing a portion of the building frame at the interior joint between the column and beams, as shown in Fig. 2(a). Figure 2(b) demonstrates the bending moments diagram of a laterally loaded moment resisting frame. In Fig. 2(c), maximum bending moments occur at the connection where the shear force is also at a maximum. Test specimens were subjected to lateral cyclic loads and concentrated load H at the top of the upper column as shown in Fig. 2 (d) so that the bending moment and shear forces were reversed and cycled. Thus, the distribution of the bending moment in the specimens was the same as for the moment-resisting frame under cyclic loading.

In this study, both beam ends and the bottom of the lower column were supported by the mechanical hinges. Several LVDTs were installed to measure displacements of the test specimen during the experiment as shown in Fig. 3 (a). Also, the strain profile of the steel reinforcement in the test specimens was observed by strain gauges. The locations of the strain gauges are shown in Fig. 3(c). Quasi-static cyclic testing was used to observe the structural response. The quasi-static lateral loading (H) was applied by a hydraulic actuator at the top of the upper column. The top column was pushed forward and pulled backward in a reversed cyclic pattern according to ACI T1.1-01. The loading history is shown in Fig. 3(d). A story drift ratio, defined as the ratio of the lateral displacement at the top of the column to column height, was used to represent the lateral movement of the test specimens. The drift level was increased to 0.15%, 0.20%, 0.25%, 0.35% ... drift until the test concluded. In each story drift level, the peak amplitude was applied repeatedly for three cycles. The repeated cyclic loading was done to check the stability of the hysteresis behavior. Furthermore, a constant axial load of $0.10f'_cA_g$ or 235 kN was applied vertically at the top of the column to satisfy the strong column-weak beam requirement.

3 Precast concrete connection installing process

The precast frame comprised precast beams and columns. Beam-to-beam connections used a T-section embedded into each beam and lap-splices through the concrete joints. Steel column sockets with bolted connectors were used for column-to-column connections. The precast beam generally used was a T-section that was 355 mm long embedded at the middle beam section equal to 220 mm; the other part was embedded into the joint core. Also, 2-DB12 steel bars (500 mm long) were welded at the end of the T-section with a 50 mm weld length and a 6 mm weld leg as shown in Fig. 4(a). The other part of the steel bars was embedded into the beam. Figure 4(b) illustrates the interior sub-assemblage installation process with the details of specimen P2, which were only slightly different from the other specimens. Both precast beams were setup on the top edge of the bottom column. Then, steel plates with a thickness of 8 mm (75 mm × 150 mm, width × length) were welded to connect both beams at the edges of the T-section steel. At the top beam section, the lap-splices (1300 mm long with the same top longitudinal reinforcement amount of the beam) were used to connect between the beam-to-beam and through the joints. The lap length of the spliced bars was 500 mm. The top precast column was installed by the column socket with bolted connectors. Finally, cast-in-place non-shrink grout concrete was placed into the joint core and upper part of the beams.

4 Test specimens

This study comprised one monolithic specimen and five precast concrete specimens with different connection details. The seismic performance of all precast specimens was compared to the monolithic control specimen. The geometries of the structural elements of all specimens were designed according to the strong-column/weak-beam design philosophy. The cross section of the beam was 150 mm × 300 mm. The cross section of the column was 200 mm × 300 mm. The reinforcement bars arrangement and concrete cross section are shown

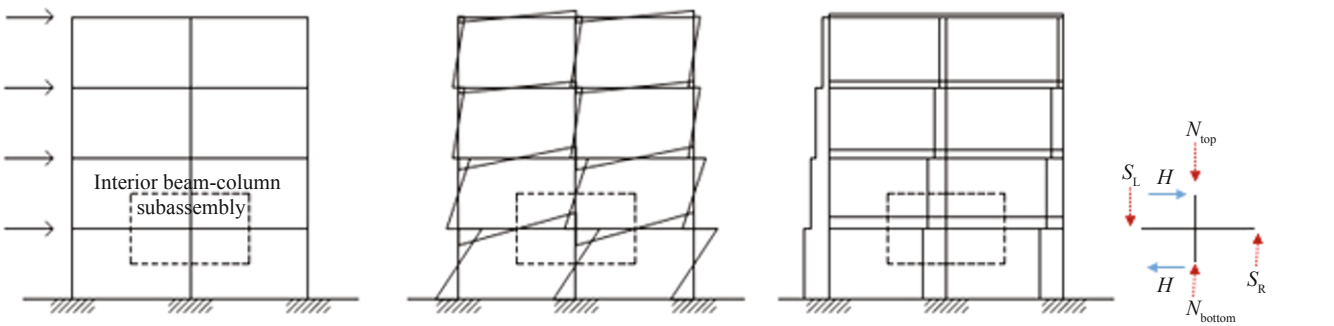

(a) Frame under lateral loads (b) Bending moment diagram (c) Shear force diagram (d) Beam-column subassembly

Fig. 2 Frame under lateral loads

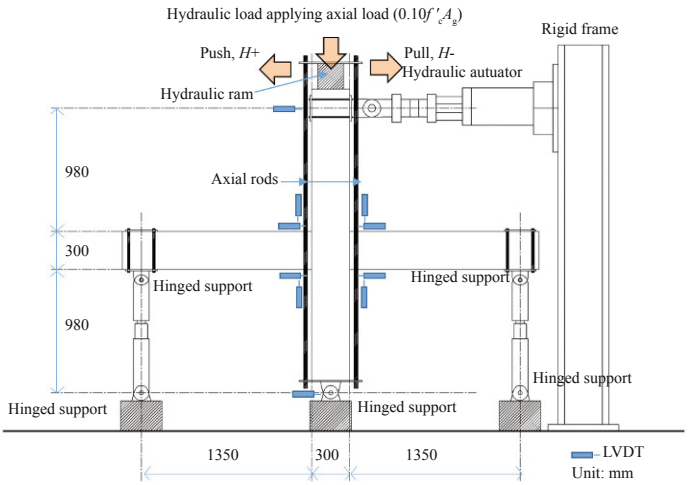

(a) Configuration of test setup

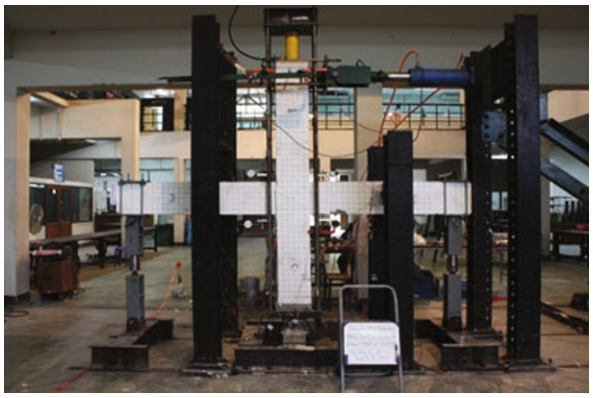

(b) View from test set up

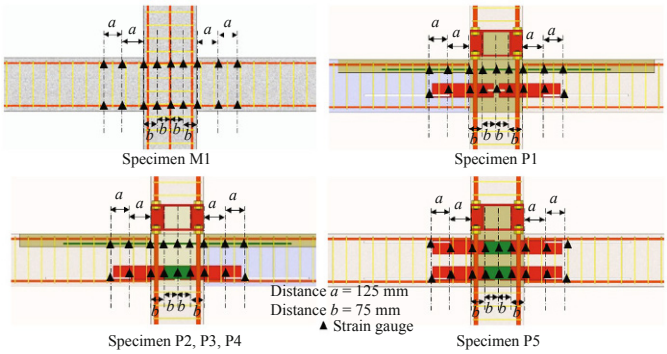

(c) Strain locations on longitudinal reinforcement

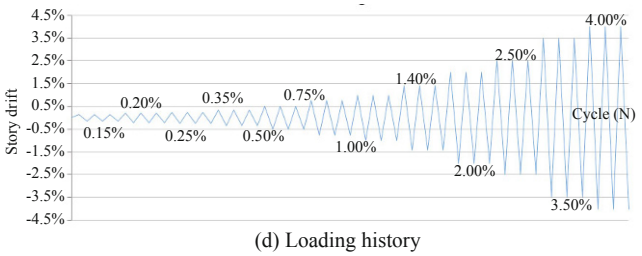

(d) Loading history

Fig. 3 Experimental setup and Loading history

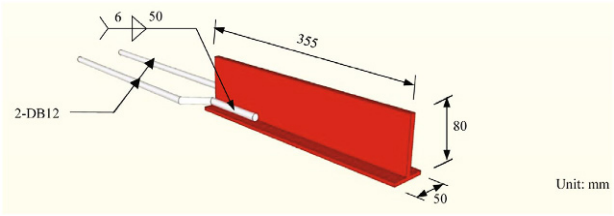

(a) T-section steel insert

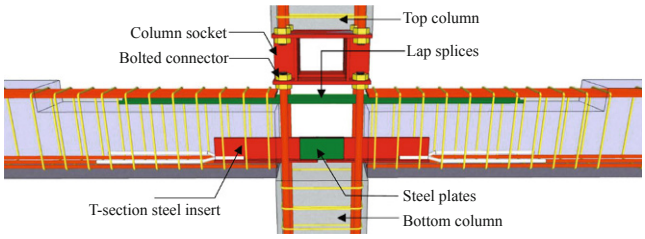

(b) T-section steel insert

Fig. 4 Precast assemblage process

in Figs. 5 and 6 for monolithic and precast specimens, respectively. Table 1 describes the joint detailing and expected strength capacity of all the specimens. The expected strength capacities were calculated according to ACI 318-14 and no bond-slip effect was considered.

4.1 Monolithic connection (M1)

The monolithic concrete specimen was designed according to ACI 318-14 and ACI 352R-02 (2002) for moderate-seismic regions. The joint detailing is shown in Fig. 7 (a). For the concrete beam, the amount of longitudinal reinforcement ratios was 0.0086 (3-DB12) and 0.0116 (4-DB12) for the bottom and the top of the beam section, respectively, and the steel reinforcement ratio of the column was 0.0118(10-DB12). Six RB6-

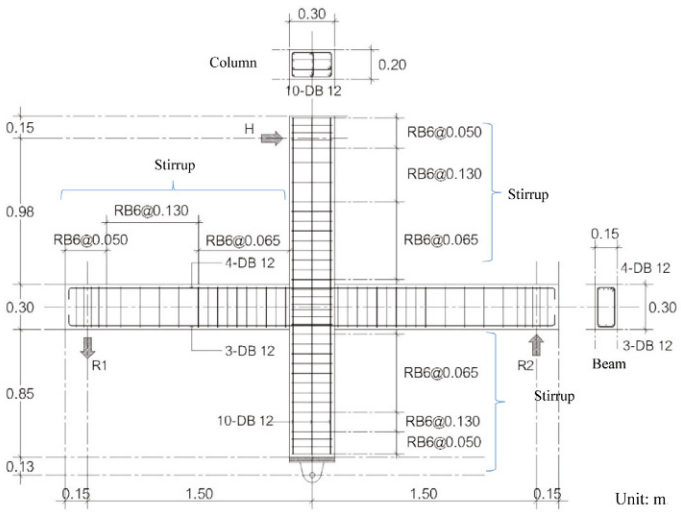

Fig. 5 Detailing of interior monolithic subassemblage frame

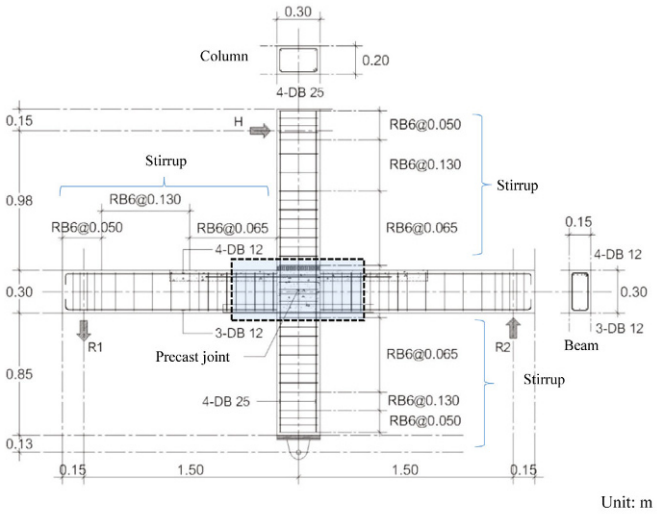

Fig. 6 Detailing of interior precast subassemblage frame

closed stirrups were contained in the concrete joint. The stirrup spacing of the beams, columns and joint are shown in Fig. 5.

4.2 Gravity precast concrete connection (P1)

The detailing of the P1 specimen was represented as a gravity resistive precast specimen. The T – section steels were located at the middle-depth of the beam section. For the connecting process, a DB-12 chain-shaped bar was input in the 15 mm diameter-holed on the T-section. About the top detailing, 4-DB12 lap-splices with the same steel ratio as the top reinforcement of the beam were used to connect the beam-beam through the joint. There was no transverse steel in the joint as shown in Fig. 7(b).

4.3 Precast concrete connection (P2)

The T-section steels were shifted down to the bottom-depth of the beam section. Moreover, the two steel plates were used to connect the T section steel inserts by the welding process, as shown in Fig. 7(c). The other connection parts were the same as the P1 specimen.

4.4 Precast concrete connection specimen (P3)

The precast connection detailing within the joint of the P3 specimen was very similar to those of specimen P2 excepting the inclusion of 5-RB6 stirrups in the column joint, as shown in Fig. 7(d).

4.5 Precast concrete connection specimen (P4)

The precast connection details within the joint of P4 specimen were developed from those of specimen P3. In addition, four DB12 diagonally bars were installed in the joint core, as shown in Fig. 7(e).

4.6 Precast concrete connection specimen (P5)

For the specimen, the lap-splice bars at the top of the beam section were replaced by using the two reversed T-section steels to connect the beam across the concrete joint. Therefore, the beam sections were symmetrical in terms of the steel reinforcement ratio. In the installation process, four steel plates were used to connect these T-sections at both the bottom and top with the welding process. The detailing of this specimen is shown in Fig. 7(f). The aim of this detailing is to relocate the splitting crack far away from the beam ends.

5 Material properties

5.1 Concrete

Normal concrete was used for the production of the test specimens. Uniaxial compressive strengths were 44.03 MPa for the monolithic one and 42.97 and 45.35 MPa for the beam and column precast elements, respectively. The mix proportion was as follows:

- Portland cement type 1: 393 kg/m^3
- Fly ash: 43 kg/m^3
- Water: 174 kg/m^3
- Sand: 824 kg/m^3
- Coarse aggregate (max size 19 mm): 914 kg/m^3
- Additional water reducing agent: 6.53 lite/m^3

Moreover, non-shrink grout concrete (Sikagrout

Table 1 Joint detail of the test specimens

Specimen	Designed parameters	Expected maximum Strength (kN)
M1	Monolithic	42.44
P1	T-section steel insert at middle layer + lap-splice bars at top beam	40.51
P2	T-section steel insert at bottom layer + lap-splice bars at top beam	50.15
P3	T-section steel insert at bottom layer + lap-splice bars at top beam + Transvers reinforcement bars	50.15
P4	T-section steel insert at bottom layer + lap-splice bars at top beam + Transvers reinforcement bars + Diagonal bars	50.15
P5	T-section steel inserts at top and bottom layers + Diagonal bars	53.05

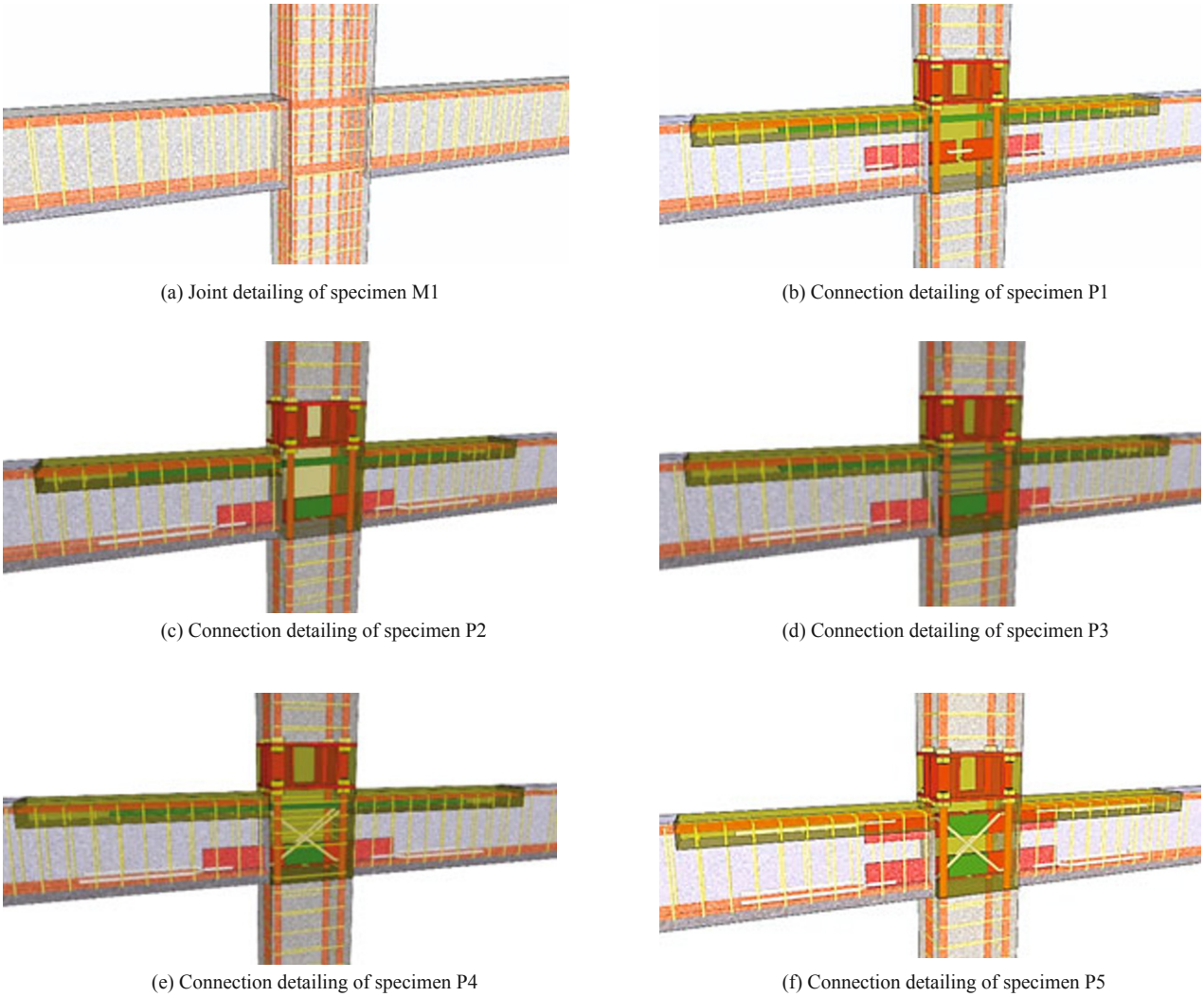

(a) Joint detailing of specimen M1

(b) Connection detailing of specimen P1

(c) Connection detailing of specimen P2

(d) Connection detailing of specimen P3

(e) Connection detailing of specimen P4

(f) Connection detailing of specimen P5

Fig. 7 Connection detailing

212-11) with a strength of 57.30 MPa was used in the precast concrete joint.

5.2 Reinforcing steel bars and steel plate

The reinforcing bars and steel plates to form a steel T-section insert were used to produce the test specimens. The uniaxial tension test was performed to investigate their mechanical properties. Table 2 shows a summary of the mechanical properties of the steel used in both the monolithic and precast specimens.

6 Test results

6.1 Crack development and failure mode

Figure 8 illustrates the crack pattern of all specimens developed from small loading to the final drift level. For all specimens, flexural cracks on the beams were first observed at the potential plastic hinge regions located at distances of *d/2* - *d* (effective beam depth) from the column faces. As the drift level increased, these cracks

Table 2 Properties of the steel used in test specimens

	Yield strength (MPa)	Ultimate strength (MPa)
RB6 (6 mm)	372	542
DB12 (12 mm)	426	572
DB25 (25 mm)	443	686
Steel plate and T-section insert	277	348

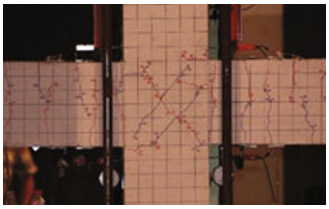
Drift ratio = 1.00%

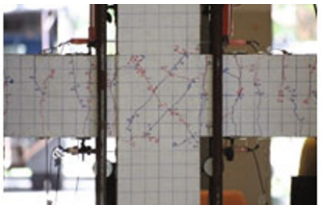
Drift ratio = 2.00%

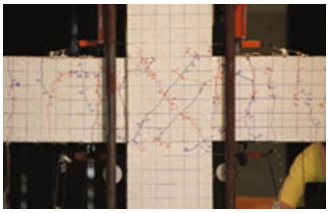
Drift ratio = 2.50%

(a) Specimen M1


Drift ratio = 1.00%

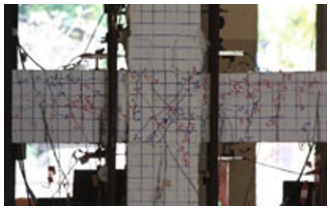
Drift ratio = 2.00%

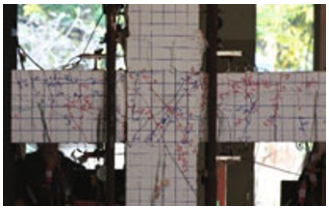
Drift ratio = 2.50%

(b) Specimen P1

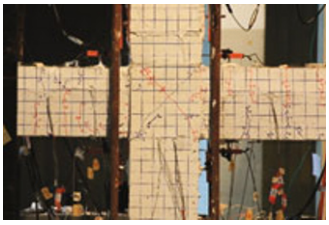
Drift ratio = 1.00%


Drift ratio = 2.00%


Drift ratio = 2.50%

(c) Specimen P2

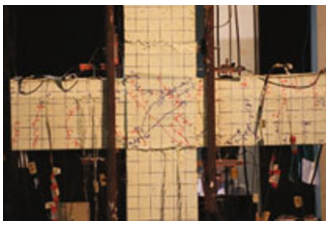
Drift ratio = 1.00%

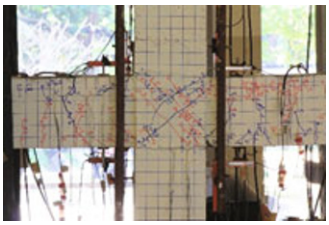
Drift ratio = 2.00%

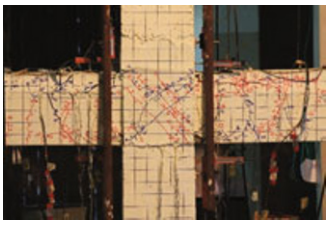
Drift ratio = 2.50% (Failure)

(d) Specimen P3

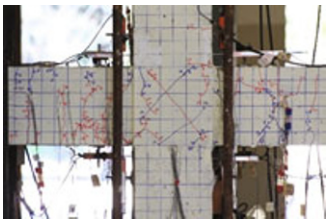
Drift ratio = 1.00%

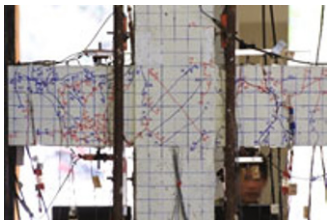
Drift ratio = 2.00%

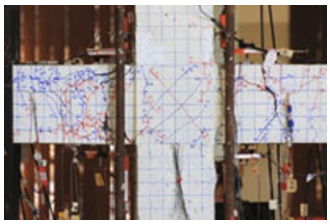
Drift ratio = 2.50% (Failure)

(e) Specimen P4

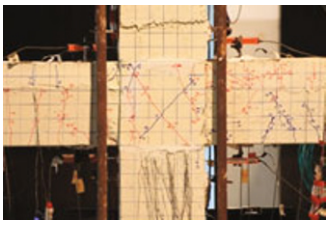
Drift ratio = 1.00%

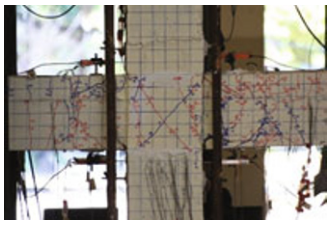
Drift ratio = 2.00%

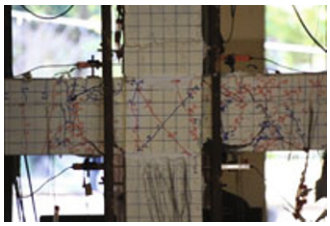
Drift ratio = 2.50%

(f) Specimen P5

Fig. 8 Crack patterns of all specimens

further propagated and a few flexural cracks also developed on the concrete columns above and below the joint region. Then, the first diagonal cracks on the beam-column joint core appeared at 0.50-0.75 % drift level. The cracking development from the drift larger than 1% of all the specimens was different due to the different reinforcement details. For the monolithic specimen M1, major cracking was the flexural cracks in the beams near the column faces and there were a few diagonal cracks within the concrete joint. Only a limited number of flexural cracks appeared in the columns immediately above or below the joint as shown in Fig. 9 (a). When the drift level reached 3.50%, crushing of the concrete cover at the bottom of the beams began and the beam bottom longitudinal bars buckled at a 4.00% drift level, as shown in Fig. 8 (a).

For the gravity precast concrete connection specimen (P1), at the 0.75% drift level, laterally splitting cracks running parallel to the T-section steel, installed at the middle beam depth, close to column face started. When the drift level was increased to 1.40%, the first splitting cracks formed at distances of *d* from the column faces along the lap-splices of the main longitudinal bars at the top section of both beams. By increasing the drift level up to 2.00-3.50%, the splitting cracks were gradually propagated and opened wider than 2.0 mm. In addition, the new flexural cracks on both beams were distinctly observed at the potential plastic hinge regions near the column face and no cracks appeared in the column. The splitting cracks at the top and middle of the beam cross section near the column face resulted in a dramatic decrease in the shear capacity. Figure 8 (b) shows the crack patterns of specimen P1 at failure.

In specimen P2, at a drift level of 1.00%, visible lateral cracks were observed at the bottom of both beams and the joint core at the beam-column interface. A few splitting cracks appeared parallel to the lap-splices and main longitudinal bars at the top beam section, which were initiated at distances of 250 mm away from the column faces. When increasing to a drift level of 1.40%, cracks gradually propagated along the lateral directions as the drift levels were increased. When the drift level reached to 3.50%, the concrete of the top beam section close to the beam-column joint started to crush and spall along the splitting crack. Similar to specimen P1, no cracks appeared on either the top or bottom columns, as shown in Fig. 8 (c).

Specimens P3 and P4 also showed similar crack patterns as P2 as shown in Fig. 8 (d-e). The main failure modes were initiated from the bond splitting cracks that occurred along the lap-splices at the top beam section in the cast-in-place grout concrete regions.

For specimen P5, as the drift level increased to 1.40%, the splitting cracks appeared parallel to the steel T-section and the main longitudinal bars were initiated at the bottom beam section, close to the column faces. With the increase in the drift level, the splitting cracks further propagated. The concrete below the T - section steel at the bottom beam section close to the beam-column joint crushed and spalled. At a distance of about the beam depth from the column face of both precast beams, the flexural cracks were very large. Figure 8 (f) shows the crack distribution of the specimens after testing.

For precast specimens P1 to P4, the major failure mode progressed from tensile splitting-cracks, which developed along the splice length at the top of the precast beam section in the non-shrink grout concrete region. That led to both slippage and strength degradation of the spliced reinforcement. From previous studies about bond behavior with high strength concrete, the loading capacity decreased rapidly after forming longitudinal spitting cracks.

A number of flexural cracks were distributed over the precast concrete beams, especially in the potential plastic hinge regions near the column, as shown in Fig. 9 (b-e). Diagonal cracks on the beam-column joint were observed. Nevertheless, no cracks appeared in the column of both the top and bottom ones of these precast specimens. Regarding specimen P1 that used a chain-shaped bar to connect both precast beams, sliding of the T-sections was observed during testing.

Figure 9 (f) shows the damage at the failure of the precast specimen P5. The specimen failed mainly by the flexural cracking in the precast beam; also, little splitting cracks were observed and both cracks were located at distances of *d* away from the precast column face. Spalling of concrete covers at the end of both beams were observed and little splitting cracks appeared at a distance of *d* from the column face.

6.2 Hysteresis behavior and strength

The relationship of lateral load against displacement at the upper column for each specimen is shown in Fig. 10. Figure 10 (a) illustrates the lateral story shear and displacement hysteresis response of the monolithic specimen. The behavior was good in terms of ductility and energy dissipation. Furthermore, no pinching effect was observed on the reversed response. The shear story showed little strength or stiffness degradation until the story drift level was up to 4.00%. Plastic hinging took place in the beams at a distance of *d*/2 from the column faces. The ultimate lateral load capacities of the monolithic one for the push side and pull side were 44.43 kN and -42.08 kN, respectively.

Regarding the P1 to P4 precast specimens, which have longitudinal lap splice bars at the top beam located at the end regions of the beams, a distance of *2d* from column face, the hysteretic load-displacement relating to the precast specimens P1-P4 are shown in Fig. 10 (b-e). As can be seen, the hysteresis's response results in the pinching effect due to the splitting crack in the top of the longitudinal lap splice bar and bond deterioration, indicating low energy dissipation. The widening of the splitting cracks in the high strength non-shrink region resulted in the dramatic degradation of the story shear

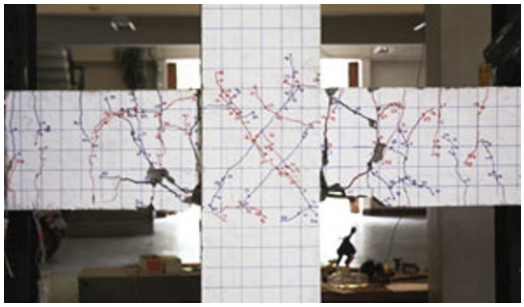

(a) Specimen M1 at 4.00 percent story drift ratio

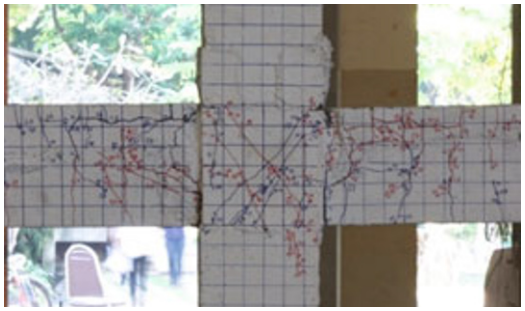

(b) Specimen P1 at 3.50 percent story drift ratio

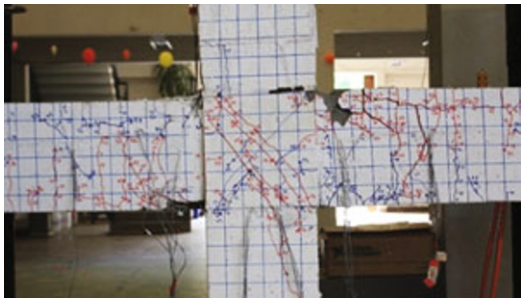

(c) Specimen P2 at 3.50 percent story drift ratio

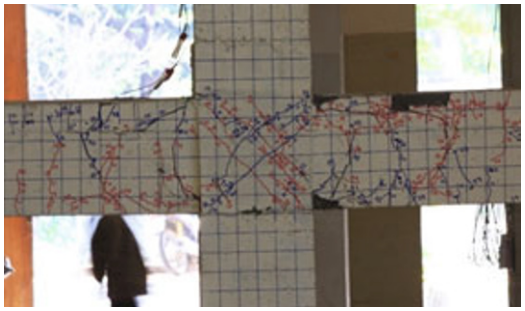

(d) Specimen P3 at 2.50 percent story drift ratio

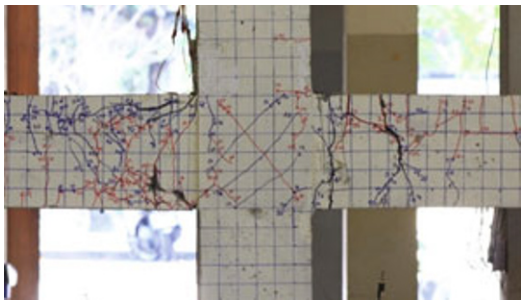

(e) Specimen P4 at 2.50 percent story drift ratio

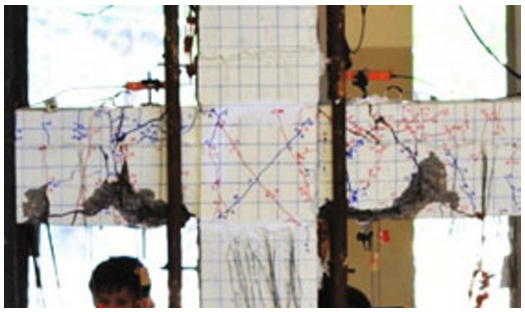

(f) Specimen P5 at 3.50 percent story drift ratio

Fig. 9 Crack distribution of test specimens at the end of testing

capacity after peak loading. These specimens showed a limited ductile response as shown in Fig. 10 (b) to Fig. 10 (e). The maximum lateral loads of these precast ones are presented in Table 3. The maximum loads of specimen P1 were lower than all the other precast specimens because the depth between the main longitudinal bars and steel T-section were lower compared with the other precast specimens.

However, the precast specimen P5, with a double T-section installed into the top and bottom beam section, located within distance *d* from the column faces, behaved satisfactorily. The hysteresis behavior of the specimen showed a little pinching during the reversible load testing and considerable pinching effect occurred in the precast specimen due to the observed flexural failure in the precast beams. The failure mode represents the successful relocation of the plastic hinge in the beams. The behavior of this specimen was good in terms of ductility and energy dissipation when compared with other precast ones. The peak recorded lateral loads were 40.92 kN and 36.42 kN for the push side and the pull side, respectively. The column story shear versus drift ratio of the specimen P5 is shown in Fig. 10 (f); the envelope curve shows that the strength degradation was rapid at the post peak strength.

The test results for the ultimate strength of all the specimens are shown in Table 3. It can be seen that the maximum strength of the monolithic specimen was close to the expected ultimate strength. For all precast specimens, the ultimate strengths were lower than the expected maximum strength and the average maximum strength of the monolithic specimen because the splitting cracks along the splice length in the high strength non-shrink region appeared during experiment. That led to both slippage and bond degradation of the overall frame specimens.

6.3 Strain distribution

All specimens obviously exhibited a strong column-weak beam mechanism. Therefore, the longitudinal reinforcement of the beam at the top and bottom of

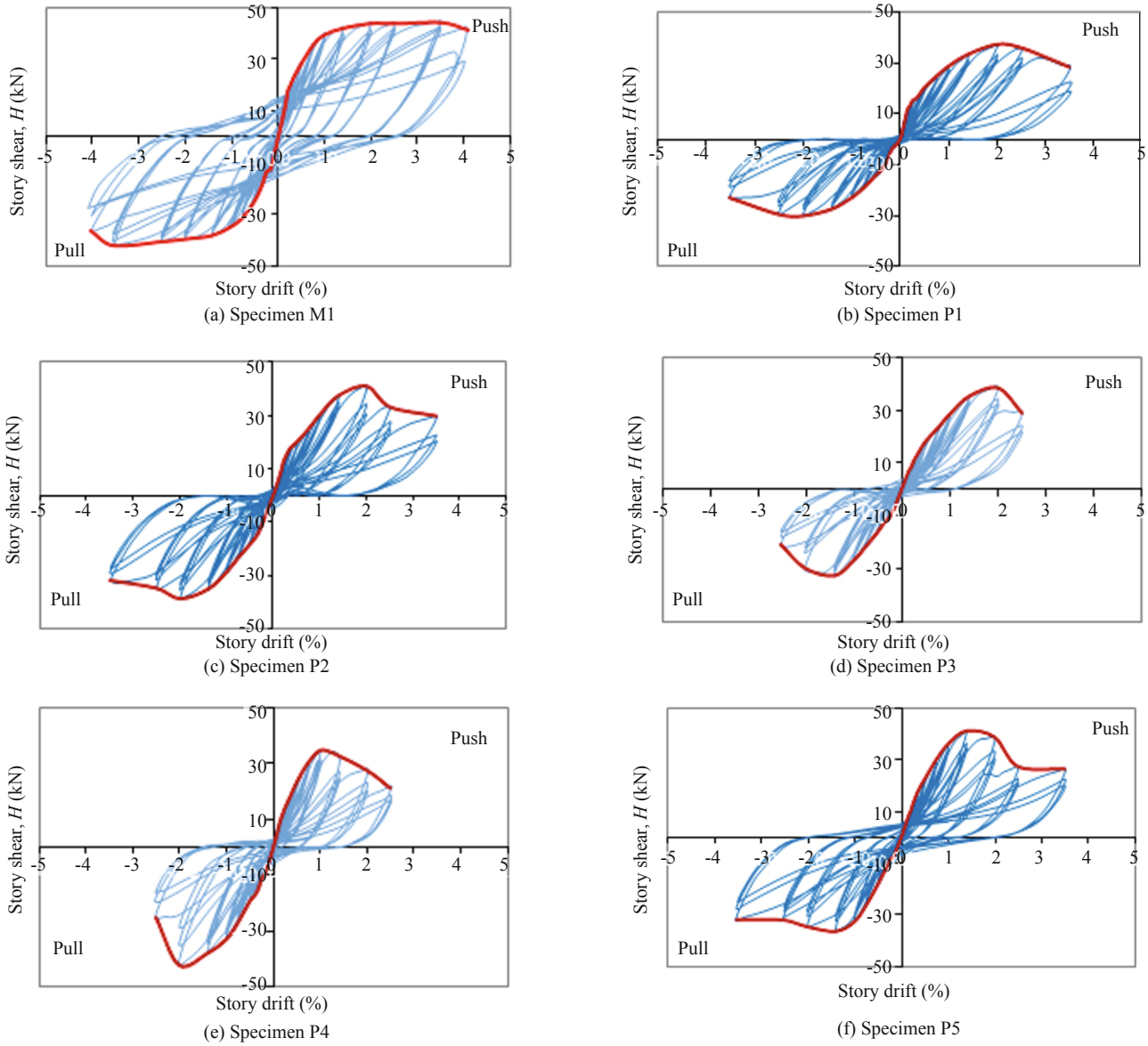

Fig. 10 Story shear force vs. story drift ratio of test specimens

Table 3 Ultimate strength and story drift level at peak of story shear

Specimen	Push Side (H+) Ultimate strength (kN)	Pull Side (*H*-) Ultimate strength (kN)	Average Ultimate Strength (kN) H_{avg}	Expected Ultimate Strength (kN) H_{expect}	Ratio of $\frac{H_{avg}}{H_{expect}}$
M1	44.43	42.08	43.25	42.44	1.02
P1	36.99	30.09	33.54	40.51	0.83
P2	40.91	38.81	39.86	50.15	0.79
P3	38.52	32.63	35.58	50.15	0.71
P4	34.98	42.23	38.61	50.15	0.77
P5	40.92	36.42	38.67	53.05	0.73

the joint region were a critical location during the experiment. The strain profiles at story drift levels of 1.00% and 2.50%, the yield point and the ultimate point of most precast specimens, are explained herein. The Fig. 11 shows the strain profile of the reinforcement in the critical region at the story drift levels of 1.00% and 2.50%.

At the story drift level of 1.00% as the yield point of the test specimens, only the reinforcement of monolithic specimen M1 rose to the yield strain level. Also, the strain levels of the top and bottom reinforcement of specimen M1 were up over the yield level at the beam plastic hinge zone, at 2.50% story drift. For precast specimens, the strain profiles of all precast specimens were under the yield level, at 1.00% drift level. For the strain levels of the top reinforcement compared to the yield strain of the steel bar at the story drift level of 2.50%, the P1 and P3 specimens were higher but the P2 and P4 specimens were lower. For the P5 specimen, the strain levels were climbed to over the yield level at both the T-section steel and the embedded steel bar at the edge of the T-section. For the bottom reinforcement with the T-section steel insert of all precast specimens, the levels of the reinforcement were higher than the yield level.

6.4 Ductility

The backbone curve of all specimens shown in Fig. 12 was obtained to determine the strength and displacement ductility. The definition of equivalent yield (d_y) and ultimate displacement (d_u) as proposed by Park (1989) for the general case of lateral load-displacement responses was adopted in this study of the ductility factor. The ultimate displacement was taken as the post peak displacement with a 15 percent drop off in the maximum lateral load capacity, or the strength of the second/third cycle decreased over 15 percent of the first cycle.

The results are shown in Table 4 with a yield point of all specimens of around 1.00 percent story drift. Regarding the precast specimens, degradation of story shear was observed to start at a story drift of 1%-2%. The strength degradation suddenly decreased due to bond deterioration from the splitting crack of the T-section inserts and/or lap-splices in the beam near the precast column face. The precast P5 specimen showed better ductility because the plastic hinge of the beams was relocated from the beam ends to a distance away from the column faces.

6.5 Stiffness degradation

In this study, stiffness degradation was discussed based on the secant stiffness. The secant stiffness (K_{sec}) of any drift ratio, which was calculated from the peak of the pulling side to the peak of the pushing side of the last loading cycle (third cycle) as shown in Fig. 13, divided by the corresponding lateral displacement (d_1+d_2). The

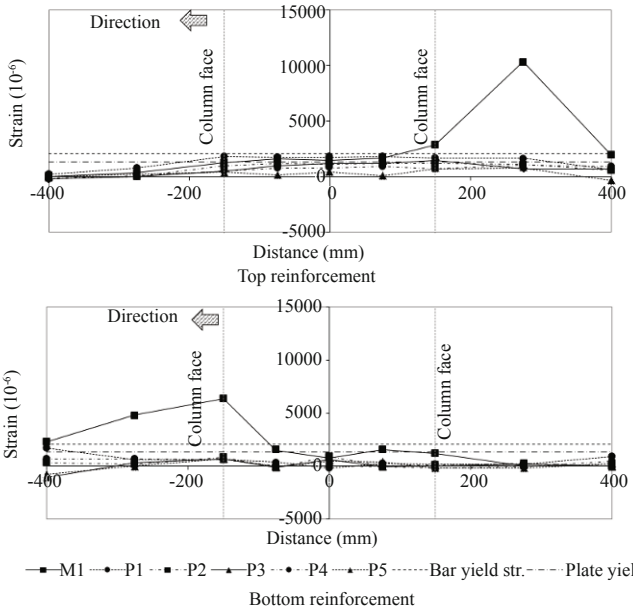

(a) Strain profile of reinforcing bar at +1.00% drift level (Push direction)

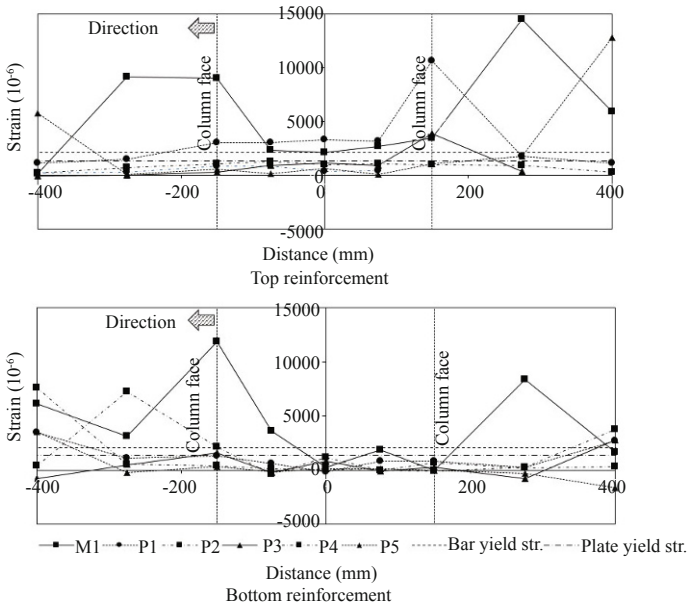

(b) Strain profile of reinforcing bar at +2.50% drift level (Push direction)

Fig. 11 Strain distribution of longitudinal reinforcement over the beam

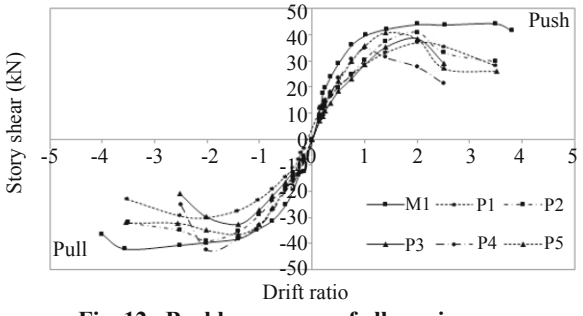

Fig. 12 Backbone curve of all specimens

Table 4 Ductility, strength and story drift level at peak of story shear

Specimen	Ductility	Push Side (H+)		Pull Side (H-)		Average strength ratio*
		Strength (kN)	Story drift (%)	Strength (kN)	Story drift (%)	
M1	4+	44.43	3.50	42.08	3.50	1.00
P1	2.47	36.99	2.00	30.09	2.00	0.77
P2	2.21	40.91	2.00	38.81	2.00	0.92
P3	1.84	38.52	2.00	32.63	1.40	0.82
P4	2.15	34.98	1.00	42.23	2.00	0.90
P5	2.62	40.92	1.40	36.82	1.40	0.90

* Ratio between strength of corresponding specimen to monolithic control specimen (M1)

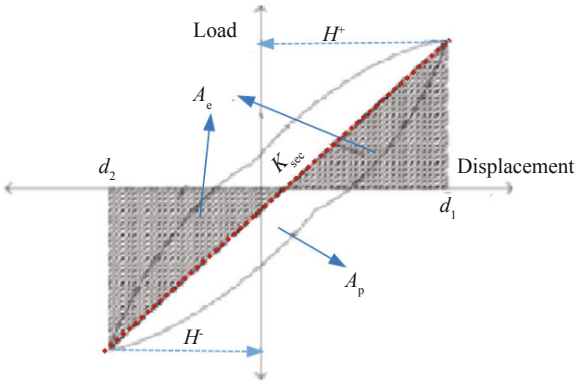

Fig. 13 Secant stiffness and equivalent damping ratio

secant stiffness value for each drift ratio was normalized (K_{norm}) by the secant stiffness at the 0.15 percent story drift, at the first drift level.

At a lower load, as shown in Fig. 14, the specimen M1 shows higher stiffness degradation compared to the precast specimens. However, the degradation rate is decreased for the precast specimens, the steel inserts increase the stiffness and control cracking well at a lower load, especially for specimen P5. However, when the critical crack was presented, the capacity suddenly decreased along with stiffness degradation.

6.6 Equivalent viscous damping ratio

In this study, the equivalent viscous damping ratio (ζ_{eq}) proposed by Chopra (2011) was used to explain the energy dissipation characteristics. The equivalent damping ratio was computed from the enclosed area within the hysteresis loop divided by strain energy, which is calculated from the assumed linear elastic behavior at corresponding cycles. This definition is formulated in Eq. (1).

$$\zeta_{eq} = \frac{1}{2\pi}\frac{A_p}{A_e} \times 100 \quad (1)$$

The equivalent viscous damping ratio versus story drift level of all test specimens is shown in Fig. 15. The equivalent damping of the monolithic specimen M1 was higher than all the other precast ones. For the precast specimens, specimen P5 showed the best damping performance when compared with the monolithic specimen M1. At the drift level of 2.50%, other precast specimens P1, P2, P3 and P4 were obviously very low when compared with the others, especially the P1 specimen, which was designed mainly for gravity loading.

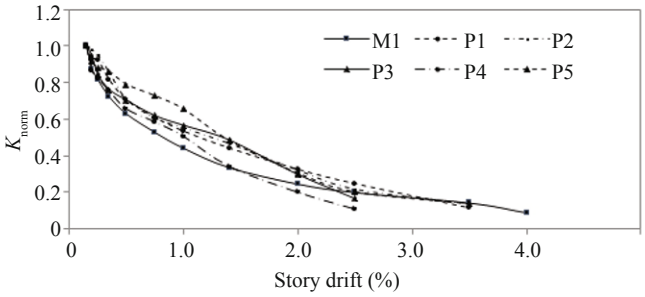

Fig. 14 Stiffness degradation

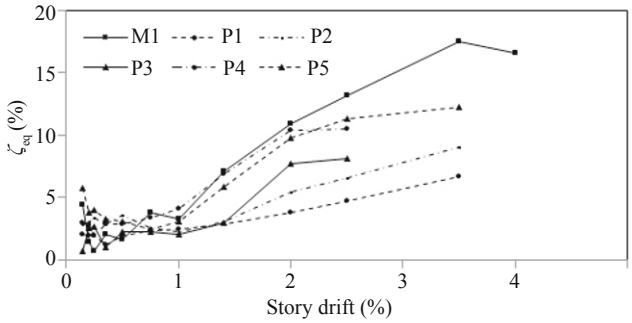

Fig. 15 Energy dissipation

7 Conclusions

The experimental results of a research study on the seismic behavior of precast concrete connections designed for earthquake resistance are presented herein. Six beam-to-column subassemblage frames were tested under cyclic loading to observe the hysteresis behavior and seismic performance of these connections. The following conclusions are drawn:

- The monolithic specimen represented seismic behavior very well. The column and joint failure was prevented by forming a potential plastic hinge at the beam ends, close to the column faces. Shear capacity, ductility, energy dissipation and stiffness degradation were very well obtained seismic parameters.
- For specimens P1-P4, the splitting crack was a major failure mode in the precast specimens. At the joint region, the top reinforcement composed of a longitudinal lapped splice with high strength non-shrink grout concrete was the weakest point. The crack developed along the splice length at the top of the precast beam section. This led to both slippage and bond degradation of the overall frame specimens.
- The maximum strength of all precast specimen was lower than the expected maximum strength because the splitting cracks along the splice length in the high strength non-shrink region appeared.
- The splitting cracks in the high strength non-shrink region resulted in the dramatic degradation of story shear capacity after peak loading.
- Regarding the equivalent damping ratio, the precast specimens with longitudinal lap splices located on the top of the joint region were obviously very low due to the formation of longitudinal spitting cracks of the lap splice.
- The precast specimen without the lap splice on the top of the joint region (P5 specimen) showed better seismic performance when compared with the other precast specimens in terms of ductility and energy dissipation, and because of that, the plastic hinge was relocated into the beams. However, the dowel bars connected to the steel inserts were too short to develop bonding.
- The design of the precast concrete beams with lap splices is needed for a longer lap length and should be done at the beam, mid span or in the low flexural stress region.

Acknowledgement

The authors acknowledge the Piboon Concrete Co., Ltd., Thailand, for providing the test samples.

References

American Concrete Institute (2001), *ACI T1.1-01. Acceptance Criteria for Moment Frames Based on Structural Testing*, Farmington Hills, MI.

American Concrete Institute (2014), *ACI 318-14. Building Code Requirements for Structural Concrete*, Farmington Hills, MI.

American Concrete Institute (2002), *ACI 352R-02. Recommendations for Design of Beam-Column Connection in Monolithic Reinforced Concrete Structures by ACI-ASCE Committee 352*, Farmington Hills, MI.

Arslan MH, Korkmaz HH and Gulay FG (2006), "Damage and Failure Pattern of Prefabricated Structures After Major Earthquakes in Turkey and Shortfalls of the Turkish Earthquake Code," *Eng. Failure Analysis*, **13**(4): 537–557.

Au FTK., Huang K and Pam HJ (2005), "Diagonally-Reinforced beam–Column Joints Reinforced under Cyclic Loading," *Structures and Buildings*, **158**(1): 21–40.

Chalioris CE, Favvata MJ and Karayannis CG (2008), "Reinforced Concrete Beam–Column Joints with Crossed Inclined Bars under Cyclic Deformations," *Earthquake Engineering and Structural Dynamics*, **37**(6): 881–897.

Chopra AK (2011), *Dynamic of Structures-Theory and Applications to Earthquake Engineering*, Prentice-Hall, Inc., Englewood Cliffs, N.J.

Diab AM, Elyamany HE, Hussein MA and Al Ashy HM (2014), "Bond Behavior and Assessment of Design Ultimate Bond Stress of Normal and High Strength Concrete," *Alexandria Engineering Journal*, **53**(2): 355–371.

Ertas O, Ozden S and Ozturan T (2006), "Ductile Connections in Precast Concrete Moment Resisting Frames," *PCI Journal*, **51**(2): 2–12.

Federal Emergency Management Agency (1998), *NEHRP Recommended Provisions for Seismic Regulations for New Buildings and Other Structures. 1997 ed. FEMA 30 and Commentary FEMA 303*, Washington, D.C.

Ghosh SK, Nakaki SD and Krishan K (1997), "Precast Structure in Region of High Seismicity: 1997 UBC Design Provision," *PCI Journal*, **42**(6): 76–93.

Gülkan P (1998), *The Ceyhan-Misis Earthquake of 27 June 1998: a preliminary engineering reconnaissance report. Technical Report, Middle East Technical University Disaster Management*, Implementation and Research Center, Ankara, Turkey.

Hansapinyo C (2012), "Exterior Cast-in-Place and Welded Precast Concrete Frames under Cyclic Loading," *Proceeding of the 1st Australasia and South-East Asia Structural Engineering and Construction Conference* (*ASEA-SEC-1*), Perth, Australia.

Hansapinyo C, Buachart C and Wongmetha P (2017), "Cyclic Performance of Precast Concrete Columns Using Steel Box Connection," *International Journal of Civil Engineering*, **15**(4): 663–676.

International Conference of Building Officials (1997), *1997 Uniform Building Code Volumes. II*, Whittier, CA.

Ketiyot R and Hansapinyo C (2012), "Cyclic Behavior of Exterior Precast Concrete Beam Column Frames Using Combined Welded-Bolted Connection," *Proceeding of the 1st International Conference on Performance-Based and Life-Cycle Structural Engineering*, Hong Kong, China.

Korkmaz HH and Tankut T (2005), "Performance of a Precast Concrete Beam-to-Beam Connection Subject to Reversed Cyclic Loading," *Engineering Structures*, **27**(9): 1392–1407.

Li B, Kulkarni SA and Leong CL (2009), "Seismic Performance of Precast Hybrid-Steel Concrete Connections," *Journal of Earthquake Engineering*, **13**(5): 667–689.

Lu X, Urukap TH, Li S and Lin F (2012), "Seismic Behavior of Interior RC Beam-Column Joints with Additional Bars under Cyclic Loading," *Earthquakes and Structures*, **3**(1): 37–57.

NEHRP Seismic Design Technical Brief No. 1, *Seismic Design of Reinforced Concrete Special Moment Frame: A Guide for Practicing Engineers*, USA, 2008.

Parastesh H, Hajirasouliha I and Ramezani R (2014), "A New Ductile Moment-Resisting Connection for Precast Concrete Frames in Seismic Regions: An Experimental Investigation," *Engineering Structures*, **70**(1): 144–157.

Park R (1989), "Evaluation of Ductility of Structures and Structural Assemblages from Laboratory Testing," *Bulletin of the New Zealand National Society for Earthquake Engineering*, **22**(3): 155–166.

Park R (2002), "Seismic Design and Construction of Precast Concrete Buildings in New Zealand," *PCI Journal*, **47**(5): 60–75.

Prestressed Concrete Institute (1973), *PCI Manual: Design of Connections for Pre-cast Prestressed Concrete*, Chicago, IL.

Prestressed Concrete Institute (2010), *PCI Design Handbook: Precast and Prestressed Concrete. 3rd ed.*, Chicago, IL.

Shariatmadar H and Zamani Beydokhti E (2014), "An Investigation of Seismic Response of Precast Concrete Beam to Column Connections: Experimental Study," *Asian Journal of Civil Engineering*, **15**(1): 41–59.

Soroushian P, Choi KB, Park GH and Aslani, F (1991), "Bond of Deformed Bars to Concrete: Effects of Confinement and Strength of Concrete," *ACI Mat. Journal*, **88**(03): 27–232.

Tsonos AG, Tegos IA and Penelis GG (1992), "Seismic Resistance of Type-2 Exterior Beam–Column Joints Reinforced with Inclined Bars," *ACI Structural Journal*, **89**(1): 3–12.

Vidjeapriya R and Jaya KP (2012), "Experimental Study on Two Simple Mechanical Precast Beam-Column Connections under Reverse Cyclic Loading," *Journal of Performance of Constructed Facilities*, **27**(4): 402–414.

Wongmatar P, Hansapinyo C and Buachart C (2015), "Relocation of Plastic Hinge of Interior Beam-Column Connections with Intermediate Bars in Reinforced Concrete and T-section Steel Inserts in Precast Concrete Frames," *Proceeding of the 17th International Conference on Civil, Environmental and Infrastructure Engineering: ICCEIE 2015*, Dubai, UAE.

Xue W and Yang X (2010), "Seismic Tests of Precast Concrete Moment-Resisting Framers and Connections," *PCI Journal*, **55**(3): 102–121.

Yang KH, Oh MH, Kim MH and Lee HC (2010), "Flexural Behavior of Hybrid Precast Concrete Beams with H-Steel Beams at Both Ends," *Engineering Structures*, **32**(9): 2940–2949.